Front. Optoelectron. 2015, 8(2): 220–228
DOI 10.1007/s12200-015-0490-2

RESEARCH ARTICLE

Optimised synthesis of close packed ZnO cloth and its applications in Li-ion batteries and dye-sensitized solar cells

Yue QIAN (✉), Rong LIU, Xiujuan JIN, Bin LIU, Xianfu WANG, Jin XU, Zhuoran WANG, Gui CHEN, Junfeng CHAO

Wuhan National Laboratory for Optoelectronics (WNLO), Huazhong University of Science and Technology, Wuhan 430074, China

Abstract Close packed ZnO nanoparticles on carbon cloth were synthesized by repeating a facile hydrothermal route in this study. After characterized by X-ray diffraction (XRD) and scanning electron microscopy (SEM), the obtained ZnO cloth was further studied for the applications in lithium (Li)-ion batteries (LIBs) and dye-sensitized solar cells (DSSCs). When ZnO cloth annealed at 400°C for 2 h were used as anodes of LIBs, it exhibited high capacity of 600 mAh/g and outstanding cycling capability without significant fading after 130 cycles. Moreover, it was also found that our electrodes displayed good stabilities under various humidity and temperature. Furthermore, the obtained composites were calcined at higher temperature (800°C) to remove carbon and white pure ZnO cloth was formed. We transferred the as-formed ZnO cloth to fluorine-doped tin oxide (FTO) substrate to make DSSCs, exhibiting an improved efficiency of around 0.38% assisted by $TiCl_4$ treatment.

Keywords lithium-ion batteries (LIBs), dye-sensitized solar cells (DSSCs), ZnO nanoparticles, carbon cloth, facile hydrothermal route

1 Introduction

Over the past few years, great attentions have been paid to the high-performance energy-storage and energy-conversion devices because of the growing energy crisis and environmental problem [1–4]. As an important energy-storage device, lithium (Li)-ion batteries (LIBs) have attracted worldwide attentions because they acted as the main power for various applications ranged from mobile devices to electric vehicles (EVs)/hybrid electric vehicles (HEVs) [5–8]. Also, as one promising device for inexpensive, large-scale solar energy conversion, dye-sensitized solar cells (DSSCs) have attracted a great deal of interest, as they offer high energy-conversion efficiencies at low cost [9–11]. However, for most of the electrodes for LIBs and DSSC, the existing large part of the electro-active materials surface which is invalid and blocked from the contact with the electrolyte would greatly decrease the conductivity of the electrode, leading to the gradually performance degradation of LIBs or the low conversion efficiency of DSSC [12–14]. Besides, rapid electron transport and shortened ion diffusion path would be favorable for lithium storage, and rapid electron transport and increased electron diffusion length would be beneficial to increasing the DSC dye loading [5,15]. Therefore, fabricating novel binder-free electrodes with fast electron transport and shortened ion diffusion path or increased electron diffusion length are eagerly desired for high-performance LIBs or DSSC.

It is well-known that the performances of the energy-storage or energy-conversion devices depend largely on the structures of the electrodes and the active materials [16,17]. Among the available active materials, nanostructured metal oxides have always been regarded as very appealing candidates for LIBs and DSSC because of widespread availability, intrinsically enhanced safety and low processing cost [8,18]. Among which, higher theoretical capacity of 978 mAh/g than graphite (372 mAh/g) and similar bandgap (3.37 eV) with TiO_2 (theoretical capacity is 335 mAh/g), Zinc oxide (ZnO) has already attracted a great deal of interest of researchers to study its performance in LIBs and DSSC [19–21]. However, as an anode for LIBs, nanostructured ZnO electrode suffer from the low electronic conductivity and the loss of electrical contact arising from the volume expansion during the charge-discharge process which result in capacity degradation and poor cycling performance [22,23]. Besides, nanostructured ZnO-based DSSCs exhibit low cell effi-

Received November 13, 2014; accepted March 2, 2015

E-mail: chien@hust.edu.cn

ciencies than TiO_2 nanoparticle-based DSSCs, mainly due to the recombination of injected electrons [24]. Although many efforts have been made to improve the electrochemical performance of the ZnO based energy-storage and energy-conversion devices, few attempts are succeeded.

Herein, we successfully fabricated three dimensional ZnO nanostructures by growing ZnO nanoparticles on flexible carbon cloth with high conductivity, and it was directly used as the integrated binder-free electrode for LIBs, which delivered superior electrochemical properties including high specific capacity of 600 mAh/g, excellent stability up to 130 cycles without significant capacity declining fading compared to previous reported [22,25]. The excellent electrochemical performance can be attributed to the enhanced electron transport, shortened ion diffusion path, and the enhanced electro-active surface of the active materials. Furthermore, the electrochemical performances of the batteries were also evaluated at various temperature and humidity stage for their practical applications. As demonstrated, the battery exhibits insensitive to humidity, but increased capacity with the rise of temperature and remains excellent stability at each temperature stage ranged from 20°C to 50°C, while too high temperature may give rise to the performance degradation. The ZnO microtubules assembled cloth can be obtained after the ZnO@carbon (C) cloth was annealed at 800°C for 5 h, which can be employed as the photoanode of DSSCs, exhibiting cell efficiencies of 0.31%, and 0.38% after $TiCl_4$ treatment. The results are superior to many other structural ZnO film because of the increased electron transport and electron diffusion length of the ZnO cloth assembled by criss-crossed ZnO microtubules [11].

2 Experimental materials and methods

2.1 Preparation of ZnO cloth

Flexible ZnO cloth assembled by nanoparticles has been synthesized in our groups, previously [26]. Here, by repeating the same process twice, close packed ZnO cloth was prepared. Then, the obtained ZnO cloth composites were calcined at different temperatures for possible applications in LIBs and DSSCs, respectively. Specifically, the ZnO cloth was annealed at 400°C for 2 h and used as the anodes of LIBs. And the composites were calcined at higher temperature (800°C) to remove carbon and then transferred to fluorine-doped tin oxide (FTO) substrate to make the DSSCs. It is reasonable because calcining at 800°C to remove carbon is convenient for DSSCs preparation [11], and annealing at 400°C to keep carbon cloth can enhance the stability of the specific capacity of ZnO, as carbon cloth is more stable for LIBs.

2.2 Fabrication of LIBs

The ZnO cloth, used as the working electrodes, was cut into circular plates (diameter: 8 mm) and placed at the central of anode consumable. After several drops of electrolyte consisting of 1 mol/L $LiPF_6$ in ethylene carbonate (EC) and dimethyl carbonate (DMC) (1:1 by volume) were added into, the Celgard 2400 was applied as separator to cut off the direct contact of working electrode and counter electrode (Li metal foil), followed by counter electrode, flat gasket and shrapnel stacked in order. The samples were assembled in an argon-filled glove box with the CR 2032 coin cells, and the cells were aged for about 20 h to ensure the electrodes and the membrane fully wetted by the electrolyte.

2.3 Fabrication of DSSCs

The DSSCs device was assembled according to the following routes. First, the as-synthesized ZnO powder, ethyl cellulose, ethanol and terpineol with a certain stoichiometric ratio were grinded to prepare the ZnO paste in the mortar. After the ZnO paste as binder was coated onto FTO substrate, a piece of pure ZnO cloth (1 cm × 1 cm) was transferred onto the paste. Second, the device was calcined at 500°C for 30 min to remove the organics, with the heating and cooling at speed of 1°C/min. Finally, the device was dipped in $TiCl_4$ solution (40 mmol/L) 5 times) for post-treatment at room temperature, then annealed again in air at 500°C for 30 min and subsequently sensitized in N719 ethanol solution for 6 h. These dye-loaded electrodes were assembled into solar cells with Pt-sputtered FTO counter electrodes and filled with electrolyte composed of DMPII (1.0 mol/L), LiI (0.1 mol/L), I_2 (0.12 mol/L), and 4-tert-butylpyridine (4-TBP) (0.5 mol/L) in methoxypropionitrile. The schematic structure of the device has been given in Fig. 1.

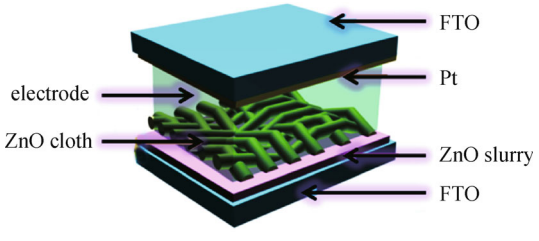

Fig. 1 Schematic structure of ZnO cloth based DSSCs

2.4 Characterizations

The composition and morphology of the materials were characterized by X-ray diffraction (XRD) and field emission scanning electron microscopy (FE-SEM, 6301). The discharge-charge cycling performances of the cells

were tested on a computer program controlled battery test instrument (LAND CT2001A). An electrochemical workstation (CH1706D) is used to collect the cyclic voltammetry (CV) curves and electrochemical impedance. Temperature and humidity programmable chamber (CZ-A-401) was used in the stability test to control the relative humidity and temperature. Photocurrent and electrochemical impedance measurements were done under AM 1.5 G conditions and with Autolab (AUT84315) respectively, with automatic data acquisition. Incident photon to current conversion efficiency (IPCE) was measured by an IPCE testing system (Newport).

3 Results and discussion

3.1 Morphology and structure characterization of ZnO cloth

X-ray powder diffraction (XRPD) was used to characterize the composition and structure of the products. Figure 2(a) shows XRPD patterns of products heat-treated at various temperatures. The materials collected without annealing show the peaks of C and ZnO, beyond that organics peaks can be also detected at 16° and 29.7°. The peaks of materials calcined at 400°C for 2 h are well matched with the standard values of ZnO (JCPDS No. 36-1451), except the information of C and ZnO, no other peaks could be detected. And we can clearly see from the curves that ZnO cloth after calcination owns good crystallinity and high purity compared to the not annealed sample. Furthermore, there are no peaks of carbon when annealed at 800°C for 5 h, which further demonstrate the carbon cloth substrate has been successfully removed. The morphology of the products was studied by using SEM. Figures 2(b) and 2(c) shows the low-magnification and high-magnification SEM images of ZnO cloth that calcined at 400°C for 2 h respectively. It is obvious that the ZnO nanoparticles are adhesive to each other together to form a compact film with rough surface after calcining, which can enhance the electrochemical active-surface and ensure the fast electronic transmission in the active materials, and then improve the specific capacity and rate capability when used as the electrode for lithium storage. Figures 2(d) – 2(f) present the SEM images of ZnO cloth, the hollow tubular structure of ZnO cloth further showed we have succeeded to remove the substrate of carbon cloths, the SEM results are matched with the XRPD patterns.

3.2 ZnO cloth as LIB anode

The electrochemical performances of our ZnO-based coin cells CR2032 were investigated in the potential range of 0.01–3V. Figure 3(a) shows the CV curves of ZnO cloth electrodes for the first three discharge-charge cycles at 0.5 mV/s. From the curves, we can clearly see that there is only one peak at the discharge process in the first cycle, which

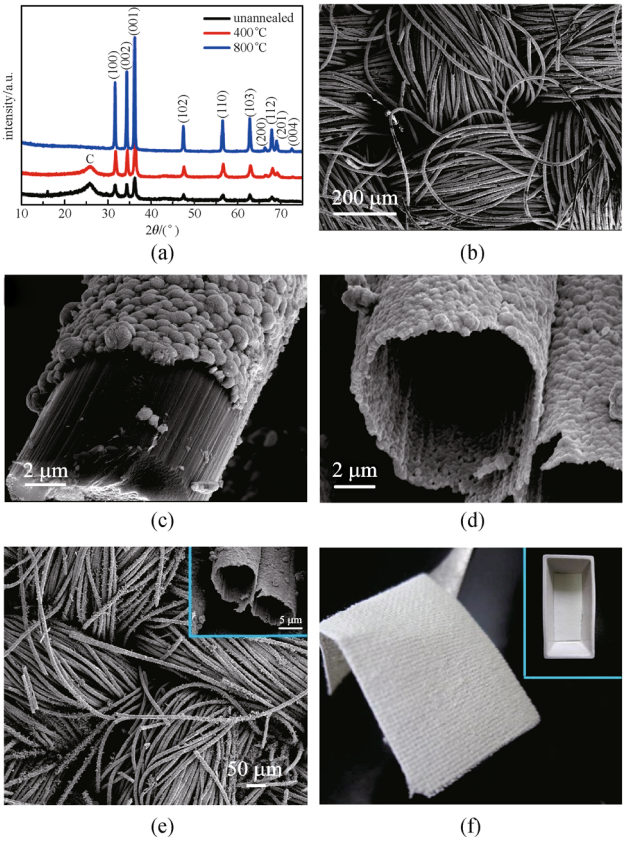

Fig. 2 (a) XRPD patterns of ZnO products at various annealing temperature; (b) and (c) SEM images of ZnO@C cloth annealed at 400°C for 2 h; (d) and (e) SEM images of ZnO cloth calcined at 800°C for 5 h; (f) ZnO cloth photo

corresponds to the reduction of ZnO, the formation of Li-Zn alloy and solid electrolyte interphase (SEI) layer. Three oxidation peaks at 0.79, 1.46 and 2.59 V are observed at the following charge curve. Two peaks at 0.79 and 1.46 V are ascribed to the multi-step dealloying process of Li-Zn alloy, and the last peak (2.59 V) corresponds to conversion of Zn to ZnO [27,28]. After the first cycle, the second cycle almost overlaps with the third one, showing high reversibility of electrode reaction.

The galvanostatic discharge-charge curves were used to further show the Li-storage performance of the as-prepared ZnO cloth assembled devices. The results of first three cycles of the cells at a current density of 200 mA/g and a voltage between 0.01 and 3 V were depicted in Fig. 3(b). The first discharge and charge capacity are 1450 and 1067 mAh/g respectively, which are both higher than the theoretical capacity for ZnO-based anodes (978 mAh/g). What's more, in the first discharge (delithiation) process, it exhibits a distinct and long plateau at 0.5 V, and is followed by a sloping curve down to the cutoff voltage of 0.01 V, which may be contributed to the formation of SEI and Li-Zn alloy reaction [20,21]. Moreover, we can see that the plateau only appears at the first cycle, because the reduction of ZnO to form Li_2O and Zn is irreversible.

The discharge capacities of the 2nd and rd cycles are 1050 and 900 mAh/g, respectively. And the corresponding regions in the charge curves attributed to the lithiation reaction can be also observed.

Additionally, the as-prepared ZnO cloth based electrodes exhibit extraordinary cyclability and stability, as evidenced in Fig. 3(c). It is encouraging to see that the capacity keeps at about 600 mAh/g without significant fading from 10 cycles to 130 cycles, the excellent electrochemical performance can be attributed to the enhanced electron transport, shortened ion diffusion path, and the enhanced electro-active surface of the active materials. Furthermore, the ZnO cloth electrodes have high coulombic efficiency of nearly 100%, which is better than that previously reported [20,21,27].

Various discharge-charge rates of these electrodes were also measured to evaluate their wonderful rate-performance, as shown in Fig. 3(d). The average specific capacities are 824, 600, 510, 300, 420 and 330 mAh/g at the current densities of 100, 200, 300, 500 and 800 mA/g respectively, and finally 770 mAh/g corresponds to the low current density 100 mA/g. Less than 7% capacity is lost after the different current densities cycled of discharge-charge process, which indicates the good reversibility of the integrated electrodes. Though the capacity gradually lost with the current rate increasing from 200 to 800 mA/g, at every single current density, the specific capacities keep excellent stability.

To evaluate the feasibility of these cells, these electrodes were cycled at the various humidity and temperature. Figure 4 (a) represents the influence of humidity on the as-assembled cells. Although humidity is changed from 50% to 90%, the capacity is still a stable value (around 540 mAh/g) at room temperature, with high coulombic efficiency (nearly 100%) [29]. We further explored the affection of temperature on the cells at a constant humidity of 50%, and the relevant curves are shown in Fig. 4(b).

With temperature range from 0°C to 60°C, it is not difficult to find that Li-ion storage performs better at high temperatures than at low ones due to the increased internal resistance, which leads to the reduced capacity of Li-ion batteries [30–33]. However, as the temperature was up to 60°C, the capacity has serious decline, which suggests that though operating a battery at elevated temperatures momentarily improves performance by lowering the internal resistance and speeding up the chemical metabo-

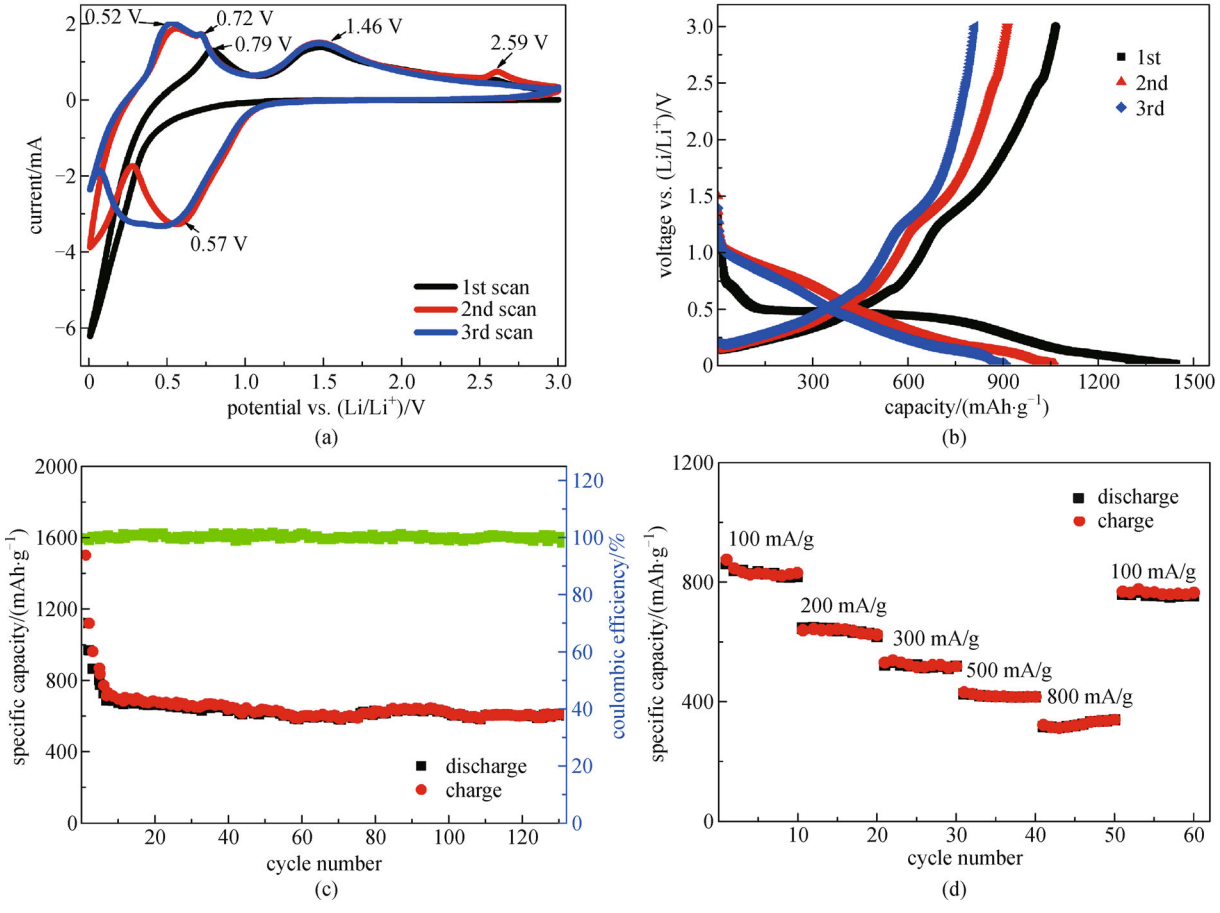

Fig. 3 Electrochemical characterization of ZnO-based half cells at the potential range from 0 to 3 V. (a) CV curves at a scan rate of 0.5 mV/s for the initial three cycles; (b) discharge-charge curves at the current density of 200 mA/g; (c) cycling performance at current density of 200 mA/g; (d) rate capacities at various current densities

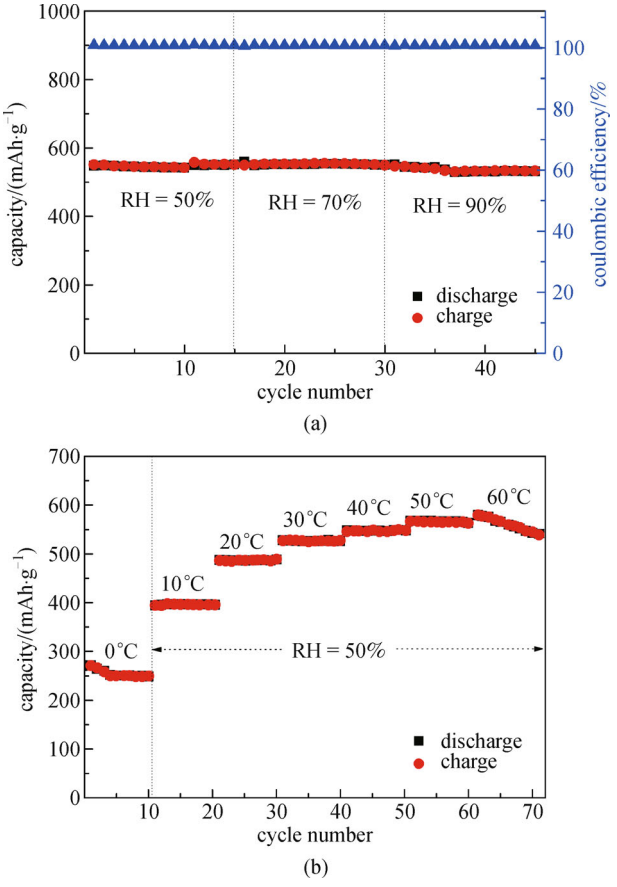

Fig. 4 Cycle performance of the battery (a) in different relative humidity (RH) at 20°C with a current density 200 mA/g; (b) in various temperatures at a constant humidity of 50% under the current density of 200 mA/g

lism, there still has a deadline that cells will be destroyed in such conditions.

To probe the kinetic properties of the ZnO cloth based LIBs, we took the electrochemical impedance spectroscopy (EIS) measurements, and the results of non-cycled and 50th cycle are shown in Fig. 5(a). The equivalent circuit model of the studied system is also shown in Fig. 5(b) according to the works reported by others [34–36]. R_s represents the internal resistance of the test battery, R_f and CPE1 are associated with the resistance and constant phase element of the SEI film, R_{ct} and CPE2 are correlated with the charge-transfer resistance and constant phase. As shown in Fig. 5(a), the first semicircle in the high-frequency region is correlated to Li-ion diffusion through the SEI layer, the second semicircle in the middle-frequency region represents charge-transfer resistances (R_{ct}), which corresponds to the charge transfer resistance and interfacial capacitance between the electrode and electrolyte, and the slopping line in the low-frequency region is related to solid state diffusion of Li-ion in the bulk electrode. The fitted impedance parameters are listed in Table 1. It can be seen that the SEI film resistance R_f and charge-transfer resistance R_{ct} of the non-cycled are 6.71 and 36.41 Ω, which are significantly lower than those of 50th cycle (7.03 and 63.29 Ω). From the result, we can conclude that the inside of cells has been changed after cycled compared with the non-cycled, the same results have been reported before [37–39].

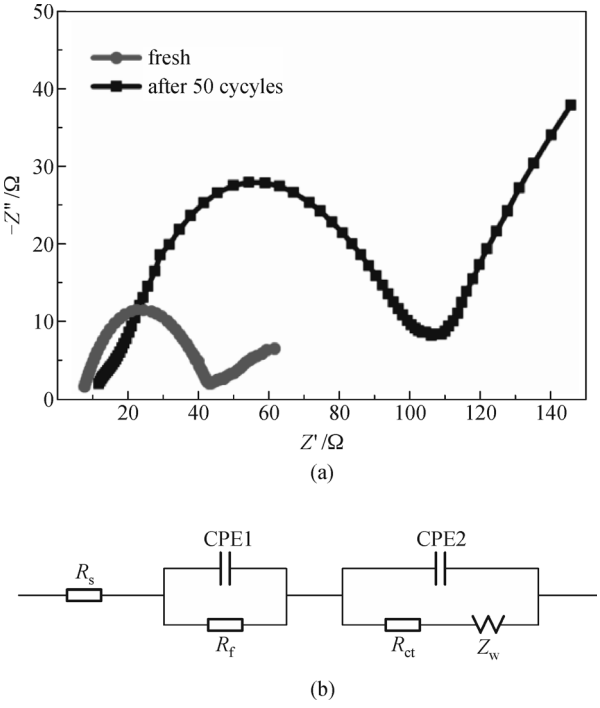

Fig. 5 (a) Impedance plots of ZnO at different cycling stages; (b) equivalent circuit model of the studied system. Z': real part of impedance; Z'': image part of impedance; Z_w: Warburg impedance

3.3 ZnO cloth as the active material of DSSCs electrode

To comprehensively understand the features and applications of the as-prepared ZnO materials in the field of energy storage and conversion, further we used ZnO cloth as electrodes of DSSCs to exploit the property of ZnO cloth in energy conversion, after we investigated the performance of ZnO-based lithium-ion battery for energy storage.

Solar cells with electrodes without and with surface treatment of $TiCl_4$ were measured under the AM 1.5 solar simulator with an illumination intensity of 100 mW/cm^2. The photocurrent density-voltage (J-V) characteristics of DSSCs are presented in Fig. 6(a). The resultant photovoltaic parameters are summarized in Table 2, and the relationship between performance parameters for the solar cells, such as open-circuit voltage (V_{oc}), short-circuit current density (J_{sc}), fill factor (FF), maximal power output (P_{in}) and conversion efficiency (η) can be expressed as the following equation:

$$\eta(\%) = (J_{sc} \times V_{oc} \times FF)/P_{in} \times 100.$$

Table 1 Fitting results of Nyquist plots using the equivalent circuit

sample	R_s/Ω	R_f/Ω	CPE1		R_{ct}/Ω
			T	P	
fresh	0.699	6.71	3.11E−5	0.719	36.41
after 50 cycles	1.281	7.03	2.44E−5	0.763	63.29

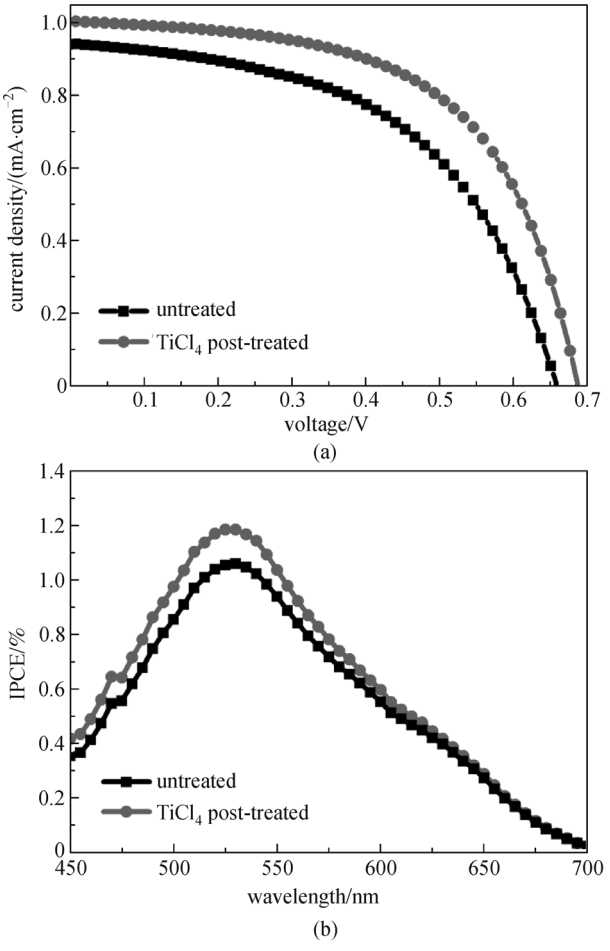

Fig. 6 (a) Photocurrent-voltage curve of DSSCs based on ZnO cloth with and without $TiCl_4$ post-treatment under AM 1.5 solar simulator; (b) IPCE spectra of $TiCl_4$ treated and untreated

And all the cell performance parameters could be gained from the *J-V* curves. As reported $TiCl_4$ solution surface treatment is beneficial to increase the amount of adsorbed dye, enhance electron transport properties and restrain charge recombination so that it can optimize the cell performance [40]. The results of Table 2 shows that, in comparison with the untreated sample, the DSSC after $TiCl_4$ post-treatment garnered the improvements of 3.03%, 6.38%, 9.62% at V_{oc}, J_{sc} and *FF* value respectively. This directly gives rise to conversion efficiency η enhanced about 22.58%.

To obtain more information about the performance of ZnO based DSSCs, IPCE spectra were tested and the results are shown in Fig. 6(b). It is seen that the $TiCl_4$ post-treated devices exhibit superior IPCE values compared to the devices build on the $TiCl_4$ untreated one. The IPCE value at 530 nm for the post-treated DSSC was 1.2%, which was higher than the untreated one of 1.06%. As we know, IPCE is determined by light-harvesting efficiency of the dye, electron injection efficiency, and charge collection efficiency, which can be affected by the morphology and surface area of the photoanode to a certain degree [41,42]. Since $TiCl_4$ treatment can modify the surface of photoanode, enhance dye anchoring ability and own much faster charge transport path, the electron injection efficiency of $TiCl_4$ post-treated devices were remarkably enhanced [19,40].

To further clarify the internal resistance and electron transfer kinetics of DSSCs fabricated with ZnO photoanodes. The EIS was measured at V_{oc} under dark. In general, three semicircles will be found in the Nyquist plots in DSSCs, while only two cycles were observed obviously in our experiments due to the poor electrical contact [41,42]. The semicircles at high and low frequencies represent the electrochemical reaction resistance at Pt counter electrode and charge transfer resistance at the ZnO/dye/electrolyte interface respectively. We define the high frequency region's resistance as R_{Pt} and the low frequency part is R_{ct}, which have been analyzed by the equivalent electrical circuit presented in the inset figure of Fig. 7. And it can be seen that the R_{Pt} values of $TiCl_4$ untreated and treated samples are 1890 and 2250 Ω respectively. The C_{Pt} value of $TiCl_4$ post-treated cell is 72.1 μF/cm^2,which is 10 times more than the C_{ct} value of untreated one of (7.2 μF/cm^2). According to the formula $\tau = RC$, the $TiCl_4$ post-treated photoanode has a longer electron lifetime of 162 ms than that of the untreated one (13.6 ms). The results suggest that the electrons in treated photoanode can travel a farther distance before being captured by recombination centers than those untreated ones.

Table 2 Photovoltaic parameters of DSSCs made by ZnO cloths electrodes with and without $TiCl_4$ treatment

photoanode	V_{oc}/V	J_{sc}/(mA·cm^{-2})	*FF*/%	η/%
untreated	0.66	0.94	0.52	0.31
$TiCl_4$-treated	0.68	1.00	0.57	0.38

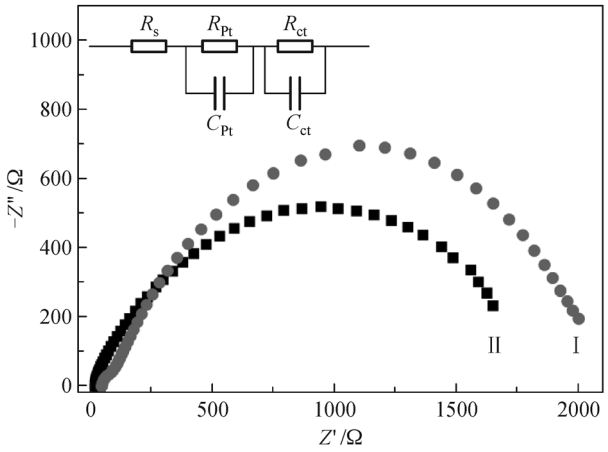

Fig. 7 Nyquist plots from impedance spectra of the ZnO photoanodes (I) with $TiCl_4$ post-treated, (II) without $TiCl_4$ treated measured at V_{oc} under dark

As a consequence, we designed a new photoanode structure for DSSC, and the device performance can be further improved because of the increased electron transport and electron diffusion length of the ZnO cloth assembled by criss-crossed ZnO microtubules, which was controlled by the $TiCl_4$ post treatment. So we carve out a new way to explore the application prospect of ZnO cloth as DSSC and have seen the silver linings about it for energy conversion.

4 Conclusions

In summary, ZnO cloth composites were fabricated via a facile hydrothermal approach. These ZnO cloth matrix can be directly used as binder-free anodes for LIBs, the as-assembled devices exhibited high capacity, excellent stability and long cycling life. After initial 10 cycles, the stable specific capacity always keep at about 600 mAh/g over 130 cycles. Besides, we also investigated the influence of humidity and temperature on these cells, they are not sensitive to the humidity but temperature can decide the destiny of capacity. Similarly, considering the novel approach of removing carbon textiles in this composite, we obtained unique ZnO cloth as photoelectrodes for high-performance DSSC with efficiency (up to 0.38%). The above results suggest that such ZnO cloth architecture is greatly potential candidate for next generation high-performance energy-storage and energy-conversion units, which opens up a novel class of ZnO-based optoelectronic devices.

Acknowledgements This work was supported by the National Natural Science Foundation of China (Grant Nos. 51002059, 21001046 and 91123008), the National Basic Research Program of China (No. 2011CB933300), the Program for New Century Excellent Talents of the University in China (No. NCET-11-0179) and the Natural Science Foundation of Hubei Province (No. 2011CDB035). Special thanks to the Analytical and Testing Center of Huazhong University of Science and Technology and the Center of Micro-Fabrication and Characterization (CMFC) of Wuhan National Laboratory for Optoelectronics for using their facilities.

References

1. Wang H, Yang Y, Liang Y, Robinson J T, Li Y, Jackson A, Cui Y, Dai H. Graphene-wrapped sulfur particles as a rechargeable lithium-sulfur battery cathode material with high capacity and cycling stability. Nano Letters, 2011, 11(7): 2644–2647
2. Guo Y, Hu J S, Wan L J. Nanostructured materials for electrochemical energy conversion and storage devices. Advanced Materials, 2008, 20(15): 2878–2887
3. Chen S, Zhu J, Wu X, Han Q, Wang X. Graphene oxide—MnO_2 nanocomposites for supercapacitors. ACS Nano, 2010, 4(5): 2822–2830
4. Wang Y, Xia H, Lu L, Lin J. Excellent performance in lithium-ion battery anodes: rational synthesis of $Co(CO_3)_{0.5}(OH)_{0.11}H_2O$ nanobelt array and its conversion into mesoporous and single-crystal Co_3O_4. ACS Nano, 2010, 4(3): 1425–1432
5. Liu B, Zhang J, Wang X, Chen G, Chen D, Zhou C, Shen G. Hierarchical three-dimensional $ZnCo_2O_4$ nanowire arrays/carbon cloth anodes for a novel class of high-performance flexible lithium-ion batteries. Nano Letters, 2012, 12(6): 3005–3011
6. Wang F, Xiang Q, Liu B, Wang L, Luo T, Chen D, Shen G. TiO_2 modified FeS nanostructures with enhanced electrochemical performance for lithium-ion batteries. Scientific Reports, 2013, 3: 2007
7. Liu J, Jiang J, Cheng C, Li H, Zhang J, Gong H, Fan H J. Co_3O_4 nanowire@MnO_2 ultrathin nanosheet core/shell arrays: a new class of high-performance pseudocapacitive materials. Advanced Materials, 2011, 23(18): 2076–2081
8. Wang Z Y, Wang Z C, Liu W T, Xiao W, Lou X W Amorphous $CoSnO_3$@C nanoboxes with superior lithium storage capability. Energy & Environmental Sciences, 2013, 6: 87–91
9. O'Regan B, Grätzel M. A low-cost, high-efficiency solar cell based on dye-sensitized colloidal TiO_2 films. Nature, 1991, 353(6346): 737–740
10. Grätzel M. Conversion of sunlight to electric power by nanocrystalline dye-sensitized solar cells. Journal of Photochemistry and Photobiology A: Chemistry, 2004, 164(1–3): 3–14
11. Wang Z, Wang H, Liu B, Qiu W, Zhang J, Ran S, Huang H, Xu J, Han H, Chen D, Shen G. Transferable and flexible nanorod-assembled TiO_2 cloths for dye-sensitized solar cells, photodetectors, and photocatalysts. ACS Nano, 2011, 5(10): 8412–8419
12. Yuan C, Li J, Hou L, Zhang X, Shen L, Lou X W D. Ultrathin mesoporous $NiCo_2O_4$ nanosheets supported on Ni foam as advanced electrodes for supercapacitors. Advanced Functional Materials, 2012, 22(21): 4592–4597
13. Wang X, Liu B, Xiang Q, Wang Q, Hou X, Chen D, Shen G. Spray-painted binder-free SnSe electrodes for high-performance energy-storage devices. ChemSusChem, 2014, 7(1): 308–313

14. Zhang G Q, Wu H B, Hoster H E, Chan-Park M B, Lou X W. Single-crystalline $NiCo_2O_4$ nanoneedle arrays grown on conductive substrates as binder-free electrodes for high-performance supercapacitors. Energy & Environmental Sciences, 2012, 5(11): 9453–9456
15. Law M, Greene L E, Johnson J C, Saykally R, Yang P. Nanowire dye-sensitized solar cells. Nature Materials, 2005, 4(6): 455–459
16. Wang G, Zhang L, Zhang J. A review of electrode materials for electrochemical supercapacitors. Chemical Society Reviews, 2012, 41(2): 797–828
17. Wang X, Liu B, Wang Q, Song W, Hou X, Chen D, Cheng Y B, Shen G. Three-dimensional hierarchical $GeSe_2$ nanostructures for high performance flexible all-solid-state supercapacitors. Advanced Materials, 2013, 25(10): 1479–1486
18. Ji L, Lin Z, Alcoutlabi M, Zhang X. Recent developments in nanostructured anode materials for rechargeable lithium-ion batteries. Energy & Environmental Sciences, 2011, 4(8): 2682–2699
19. Saito M, Fujihara S. Large photocurrent generation in dye-sensitized ZnO solar cells. Energy & Environmental Sciences, 2008, 1(2): 280–283
20. Wang H, Pan Q, Cheng Y, Zhao J, Yin G. Evaluation of ZnO nanorod arrays with dandelion-like morphology as negative electrodes for lithium-ion batteries. Electrochimica Acta, 2009, 54 (10): 2851–2855
21. Park K T, Xia F, Kim S W, Kim S B, Song T, Paik U, Park W. Facile synthesis of ultrathin ZnO nanotubes with well-organized hexagonal nanowalls and sealed layouts: applications for lithium ion battery anodes. Journal of Physical Chemistry C, 2013, 117(2): 1037–1043
22. Liu J, Li Y, Ding R, Jiang J, Hu Y, Ji X, Chi Q, Zhu Z, Huang X. Carbon/ZnO nanorod array electrode with significantly improved lithium storage capability. Journal of Physical Chemistry C, 2009, 113(13): 5336–5339
23. Belliard F, Irvine J T S. Electrochemical performance of ball-milled ZnO–SnO_2 systems as anodes in lithium-ion battery. Journal of Power Sources, 2001, 97–98: 219–222
24. Wu J, Chen G, Yang H, Ku C, Lai J. Effects of dye adsorption on the electron transport properties in ZnO-nanowire dye-sensitized solar cells. Applied Physics Letters, 2007, 90(21): 213109
25. Ahmad M, Shi Y, Nisar A, Sun H, Shen W, Wei M, Zhu J. Synthesis of hierarchical flower-like ZnO nanostructures and their functionalization by Au nanoparticles for improved photocatalytic and high performance Li-ion battery anodes. Journal of Materials Chemistry, 2011, 21(21): 7723–7729
26. Liu B, Wang Z, Dong Y, Zhu Y, Gong Y, Ran S, Liu Z, Xu J, Xie Z, Chen D, Shen G. ZnO-nanoparticle-assembled cloth for flexible photodetectors and recyclable photocatalysts. Journal of Materials Chemistry, 2012, 22(18): 9379–9384
27. Liu J, Li Y, Huang X. ZnO nanoneedle arrays directly grown on bulk nickel substrate for Li ion battery electrodes with improved performance. In: Proceedings of IEEE International Nanoelectronics Conference, 2008, 53–57
28. Liu B, Wang X, Chen H, Wang Z, Chen D, Cheng Y, Zhou C, Shen G. Hierarchical silicon nanowires-carbon textiles matrix as a binder-free anode for high-performance advanced lithium-ion batteries. Scientific Reports, 2013, 3: 1622
29. Yin H, Yu K, Peng H, Zhang Z, Huang R, Travas-Sejdic J, Zhu Z. Porous V_2O_5 micro/nano-tubes: synthesis via a CVD route, single-tube-based humidity sensor and improved Li-ion storage properties. Journal of Materials Chemistry, 2012, 22(11): 5013–5019
30. Shim J, Kostecki R, Richardson T, Song X, Striebel K A. Electrochemical analysis for cycle performance and capacity fading of a lithium-ion battery cycled at elevated temperature. Journal of Power Sources, 2002, 112(1): 222–230
31. Chiang Y, Sadoway D R, Jang Y, Huang B, Wang H. High capacity, temperature-stable lithium aluminum manganese oxide cathodes for rechargeable batteries. Electrochemical and Solid-State Letters, 1999, 2(3): 107–110
32. Wang F, Yu M, Hsiao Y, Tsai Y, Hwang B, Wang Y, Wan C. Aging effects to solid electrolyte interface (SEI) membrane formation and the performance analysis of lithium ion batteries. International Journal of Electrochemical Science, 2011, 6(4): 1014–1026
33. Wu M S, Chiang P C J, Lin J C. Electrochemical investigations on capacity fading of advanced lithium-ion batteries after storing at elevated temperature. Journal of the Electrochemical Society, 2005, 152(6): A1041–A1046
34. Song W, Xie J, Liu S, Zheng Y, Cao G, Zhu T, Zhao X. Graphene decorated with ZnO nanocrystals with improved electrochemical properties prepared by a facile in situ hydrothermal route. International Journal of Electrochemical Science, 2012, 7(3): 2164–2174
35. Wu X M, Chen S, Ma M Y, Liu J B. Synthesis of Co-coated lithium manganese oxide and its characterization as cathode for lithium ion battery. Ionics, 2011, 17(1): 35–39
36. Chang K, Chen W. L-cysteine-assisted synthesis of layered MoS_2/graphene composites with excellent electrochemical performances for lithium ion batteries. ACS Nano, 2011, 5(6): 4720–4728
37. Jia X, Chen Z, Suwarnasarn A, Rice L, Wang X, Sohn H, Zhang Q, Wu B M, Wei F, Lu Y. High-performance flexible lithium-ion electrodes based on robust network architecture. Energy & Environmental Sciences, 2012, 5(5): 6845–6849
38. Wang J, Zhou Y, Hu Y, O'Hayre R, Shao Z. Porous nanocrystalline TiO_2 with high lithium-ion insertion performance. Journal of Materials Science, 2013, 48(6): 2733–2742
39. Li J, Xiong S, Liu Y, Ju Z, Qian Y. High electrochemical performance of monodisperse $NiCo_2O_4$ mesoporous microspheres as an anode material for Li-ion batteries. ACS Applied Materials & Interfaces, 2013, 5(3): 981–988
40. Ye M, Xin X, Lin C, Lin Z. High efficiency dye-sensitized solar cells based on hierarchically structured nanotubes. Nano Letters, 2011, 11 (8): 3214–3220
41. Chang S, Li Q, Xiao X, Wong K Y, Chen T. Enhancement of low energy sunlight harvesting in dye-sensitized solar cells using plasmonic gold nanorods. Energy & Environmental Sciences, 2012, 5(11): 9444–9448
42. Zhang P, Wu C, Han Y, Jin T, Chi B, Pu J, Jian L. Low-temperature preparation of hierarchical structure TiO_2 for flexible dye-sensitized solar cell. Journal of the American Ceramic Society, 2012, 95(4): 1372–1377

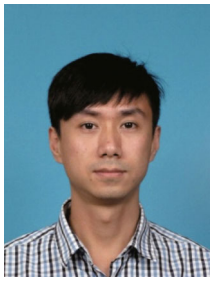

Yue Qian received the B.S. degree in optical information science and technology from Huazhong University of Science and Technology (HUST) in 2005, and the M.S. degree in test measurement technology and instrument from HUST in 2007. He is working toward his Ph.D. degree in Wuhan National Laboratory for Optoelectronics (WNLO), HUST. His research is in the area of nanoscale materials and energy storage devices.

Rong Liu received the B.S. degree in optical information science and technology from China Three Gorges University in 2011, and the M.S. degree in physical electronics from in Wuhan National Laboratory for Optoelectronics (WNLO), Huazhong University of Science and Technology (HUST) in 2014. Her research was in the area of nanoscale materials and energy storage devices.